University of Bristol - Explore Bristol Research
General rights

An impulse response function for the "long tail" of excess atmospheric CO₂ in an Earth system model

N. S. Lord[1,2], A. Ridgwell[1,2,3], M. C. Thorne[4], and D. J. Lunt[1,2]

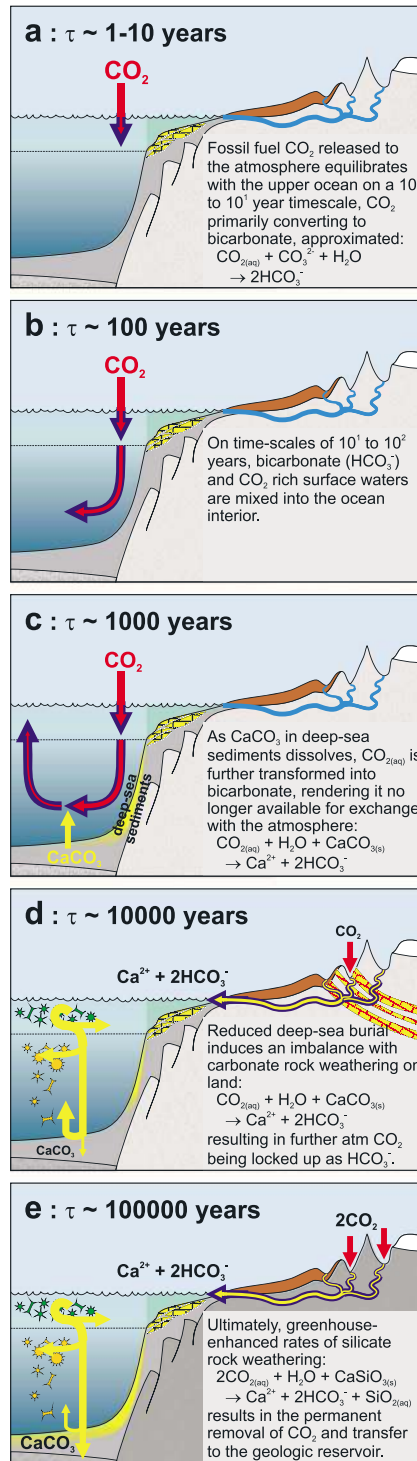[1]School of Geographical Sciences, University of Bristol, Bristol, UK, [2]Cabot Institute, University of Bristol, Bristol, UK, [3]Department of Earth Sciences, University of California, Riverside, California, USA, [4]Mike Thorne and Associates Limited, Bishop Auckland, UK

Abstract The ultimate fate of (fossil fuel) CO_2 emitted to the atmosphere is governed by a range of sedimentological and geological processes operating on timescales of up to the ca. hundred thousand year response of the silicate weathering feedback. However, how the various geological CO_2 sinks might saturate and feedbacks weaken in response to increasing total emissions is poorly known. Here we explore the relative importance and timescales of these processes using a 3-D ocean-based Earth system model. We first generate an ensemble of 1 Myr duration CO_2 decay curves spanning cumulative emissions of up to 20,000 Pg C. To aid characterization and understanding of the model response to increasing emission size, we then generate an impulse response function description for the long-term fate of CO_2 in the model. In terms of the process of carbonate weathering and burial, our analysis is consistent with a progressively increasing fraction of total emissions that are removed from the atmosphere as emissions increase, due to the ocean carbon sink becoming saturated, together with a lengthening of the timescale of removal from the atmosphere. However, we find that in our model the ultimate CO_2 sink—silicate weathering feedback—is approximately invariant with respect to cumulative emissions, both in terms of its importance (it removes the remaining excess ~7% of total emissions from the atmosphere) and timescale (~270 kyr). Because a simple pulse-response description leads to initially large predictive errors for a realistic time-varying carbon release, we also develop a convolution-based description of atmospheric CO_2 decay which can be used as a simple and efficient means of making long-term carbon cycle perturbation projections.

1. Introduction

A variety of processes, operating on timescales ranging from years to hundreds of thousands of years, act to remove excess (i.e., direct anthropogenic) CO_2 added to the atmosphere (Figure 1) and hence control its atmospheric lifetime. On the shortest, approximately annual timescales (Figure 1a), CO_2, as a soluble gas, is transferred across the air-sea interface and reacts with seawater to increase the concentration of $CO_{2(aq)}$ and bicarbonate ions (HCO_3^-), while reducing the concentration of carbonate ions (CO_3^{2-}) (and decreasing pH) [*Turley et al.*, 2010]. At the same time, modeling studies have suggested that CO_2 is taken up by the terrestrial biosphere through CO_2-driven fertilization of primary productivity [*Joos et al.*, 2001; *Schimel et al.*, 2015; *Sitch et al.*, 2008], although this theory has recently been contested by *van der Sleen et al.* [2015] who found no evidence of this effect in the analysis of the width of growth rings over the past 150 years in a number of tropical regions. On decadal to century timescales (Figure 1b), CO_2-enriched surface waters are transported down into the ocean interior [*Archer and Brovkin*, 2008; *Archer et al.*, 1998; *Sarmiento et al.*, 1992], while soil carbon stocks will tend to approach a new quasi-equilibrium with terrestrial productivity and surface temperatures.

Out beyond about a millennium from peak carbon emissions, geological processes are expected to progressively dominate the subsequent evolution of atmospheric CO_2. First, ventilation of the deep ocean with CO_2-enriched, and hence CO_3^{2-} depleted, water derived from the surface, will reduce the stability of previously deposited calcium carbonate ($CaCO_3$) in marine sediments and lead to increased rates of in situ carbonate mineral dissolution (Figure 1c), a process known as seafloor $CaCO_3$ neutralization [*Archer et al.*, 1997]. This reaction regenerates carbonate ions and hence partially restores the buffering capacity of deep waters [*Archer et al.*, 1997; *Ridgwell and Hargreaves*, 2007]. Subsequent outcropping of these waters at the surface will then enable further CO_2 uptake from the atmosphere. Furthermore, while the rate of burial of

Figure 1. Illustration of the primary mechanisms of natural sequestration of CO_2 from the atmosphere. (a and b) The pathways of carbon uptake operating on timescales of years (10^0 years) to centuries (10^2 years)—Figure 1a is air-sea gas exchange and Figure 1b is ocean invasion. (c–e) The pathways of carbon uptake occurring on timescales of millennia (10^3 years) and beyond—the "geologic" carbon sinks: Figure 1c represents the operation of seafloor $CaCO_3$ neutralization, Figure 1d represents the operation of terrestrial $CaCO_3$ neutralization, and Figure 1e represents the operation of the silicate weathering carbon sink. The red arrows represent the movement of CO_2 $_{(aq)}$, the blue arrows are HCO_3^-, and the yellow arrows represent Ca^{2+} ions. The widths of the arrows provide an indication of the relative amounts of each dissolved species. The symbols in the ocean in Figures 1d and 1e represent marine calcifying organisms living in the surface ocean (green); a proportion of which will sink and/or dissolve once dead (yellow).

$CaCO_3$ in marine sediments globally is reduced or even net negative with global dissolution exceeding supply to the sediment surface, weathering of carbonate rocks on land continues. CO_2 consumed from the atmosphere in the weathering reaction is hence no longer balanced (at long-term steady state) by precipitation and burial of new biogenic $CaCO_3$, allowing additional drawdown of CO_2 [*Lenton and Britton*, 2006; *Ridgwell and Hargreaves*, 2007]. This process has been termed "terrestrial $CaCO_3$ neutralization" [*Archer et al.*, 1997] (Figure 1d).

Finally, the residual atmospheric CO_2 perturbation is removed as a result of the response of terrestrial weathering of silicate rocks to climate (Figure 1e). In this process, a warmer, wetter (on average) climate resulting from elevated atmospheric CO_2 concentrations leads to increased weathering rates, drawing down more atmospheric CO_2 and so returning climate conditions and weathering rates back toward their unperturbed levels [*Walker et al.*, 1981]. In this paper, we choose to use the term "increased weathering",

rather than "enhanced weathering" as is often used to describe this natural climate feedback, in order to avoid confusion with the geoengineering technique of artificially increasing rates of weathering as a method of carbon capture and storage. Silicate weathering is assumed to restore atmospheric CO_2 to its original state over hundreds of thousands to millions of years [*Berner*, 1999; *Berner and Caldeira*, 1997; *Lenton and Britton*, 2006] and is responsible for the "long tail" of an atmospheric CO_2 perturbation [*Archer and Brovkin*, 2008]. Increased silicate weathering is also responsible for restoring the initial preperturbation state of ocean chemistry as on their own, seafloor and terrestrial $CaCO_3$ neutralization lead to an accumulation of both total dissolved carbon and alkalinity (Ca^{2+}) in the ocean [*Goodwin and Ridgwell*, 2010]. Increased silicate weathering can thus be viewed as being entirely responsible for the removal of carbon emissions from the surficial reservoirs, but with added carbon having been almost completely partitioned away from the atmosphere by the time silicate weathering comes to dominate the atmospheric CO_2 response.

Removal of added carbon from the ocean and atmosphere need not exclusively take place via increased silicate weathering, and other feedbacks may be important. Principal among these is organic carbon burial in marine sediments, which is thought to be enhanced under conditions of increased nutrient supply from weathering and hence marine productivity, as well as under reduced ocean oxygenation that is generally associated with a warmer climate [*Bains et al.*, 2000; *Zachos and Dickens*, 2000]. Quasi global-scale deoxygenation and enhanced carbon burial events occurring during the Cretaceous (145.5–65.5 Ma) ocean anoxic events [*Jenkyns*, 1980; *Leckie et al.*, 2002; *Schlanger and Jenkyns*, 1976] may well be a reflection of such a feedback response to episodic volcanism and global warming. However, in this study we will ignore potential additional long-term negative feedbacks and influences involving marine organic carbon burial, as well as shorter timescale interactions with the terrestrial biosphere in order to simplify the timescale analysis.

A detailed understanding of the timescales on which different global carbon cycle processes operate is essential to correctly interpret geological events, as well as to make projections of how carbon releases, such as from the combustion of fossil fuels, will affect the Earth system in the future. The timescales of operation and CO_2 uptake capacities of these processes (summarized in Figure 1) will determine the length and magnitude of the atmospheric CO_2 perturbation and consequently that of the associated changes in climate. This is of particular importance for parts of the climate system that have slow response times, such as the major ice sheets [*Stone et al.*, 2010; *Winkelmann et al.*, 2015], permafrost [*Lawrence et al.*, 2012], and marine hydrates [*Hunter et al.*, 2013; *Zeebe*, 2013]. As such, the dynamics of the long-term atmospheric CO_2 response sets the potential impact of anthropogenic emissions on future glacial-interglacial cycles [*Archer and Ganopolski*, 2005; *Berger and Loutre*, 2002].

The involvement of multiple nonlinear biogeochemical processes in determining the fate of excess atmospheric CO_2 necessitates the use of numerical model simulations, simulations which need to be of order 1 Myr in order to elucidate the complete recovery. As a consequence, box model representations of the Earth system have traditionally been developed and employed in addressing questions of long-term future [*Lenton and Britton*, 2006; *Tyrrell et al.*, 2007; *Zeebe and Zachos*, 2013] and past (geologic) [*Berner*, 1990; *Kohler et al.*, 2005; *Penman et al.*, 2014] global carbon cycling. Yet most box models lack representation of climate feedbacks that modulate the solubility of CO_2 and changes in ocean circulation (and hence transport of dissolved carbon and alkalinity). Off-line 3-D ocean circulation and carbon cycle models have been employed in making projections of the long-term response to carbon emissions but also lack an explicit climate feedback and hence have tended to assume the characteristics of the silicate weathering feedback [*Archer*, 2005; *Archer et al.*, 1997]. Even relatively computationally efficient Earth system models have generally previously only been run for a few tens of kyr [e.g., *Archer et al.*, 2009; *Meissner et al.*, 2012] and/or have not included a climate-responsive weathering feedback [e.g., *Goodwin and Ridgwell*, 2010; *Ridgwell and Hargreaves*, 2007; *Ridgwell and Schmidt*, 2010]. In one 3-D ocean-based Earth system model study to simulate the full ~1 Myr completion timescale of this feedback [*Colbourn et al.*, 2013], individual model experiments took ~2 months simulation time, and only a limited number of emissions scenarios were explored.

Because of the challenges and computational expense of spanning a full range of mechanistically represented CO_2 removal timescales in a single model, numerical response functions describing the decay of an atmospheric CO_2 perturbation have previously been developed by fitting multiple exponential decay curves to CO_2 data generated by a limited number of model experiments. For instance, *Archer et al.* [1997] derived three exponential curves from the modeled CO_2 response to a 3000 Pg C pulse emission in an off-line ocean

+ carbon cycle model. This analysis identified relaxation timescales of 365 yr, 5.5 kyr, and 8.2 kyr. The Long Tail Model Intercomparison Study performed by *Archer et al.* [2009] identified a timescale of 3–7 kyr for the process of $CaCO_3$ neutralization in a range of Earth system models of intermediate complexity (EMICs). A study by *Maier-Reimer and Hasselmann* [1987] also derived response functions for perturbation of initial atmospheric CO_2 concentrations by factors of 1.25, 2, and 4 while *Joos et al.* [2013], in a multimodel analysis of a range of models of different complexities (including comprehensive Earth system models, EMICs, and box-type models), fit a sum of three exponentials over the first 1000 years, detecting relaxation timescales of 4.3, 36.5, and 394.4 years. However, because these latter studies focused on the millennium time frame, the resulting functions are most relevant in interpreting relatively short term oceanic processes of carbon uptake such as involving atmospheric CO_2 uptake at the ocean surface and transport of dissolved carbon into the ocean interior. As part of the only explicit 1 Myr timescale analysis conducted to date, *Colbourn et al.* [2015] explored the fitting of different numbers of exponential curves and found that for a 1000 Pg C instantaneous emission, an equation consisting of the sum of six exponentials, which differ in their turn-over timescale, provided the optimum fit, capturing the timescales of shorter-term oceanic processes as well as the long-term processes. However, in an initial analysis of a 5000 Pg C release, five exponentials instead provided the best fit [*Colbourn*, 2011], raising the question of how the relative balance and respective timescale of processes and hence overall CO_2 decay dynamics might change with total carbon emissions.

The advantage of analytical treatments such as summed exponentials is that they can be applied to simulate the overall decay of a CO_2 perturbation in lieu of running a mechanistic model. The BIOCLIM project [*BIOCLIM*, 2001], for example, used the response function of *Archer et al.* [1997] to compute long-term atmospheric CO_2 following time-dependent emissions of ~3000 and ~5000 Pg C. These potential future CO_2 trajectories were then used as an external forcing in the LLN 2-D NH climate model [*Berger and Loutre*, 1996; *Gallee et al.*, 1991, 1992] to simulate the possible evolution of climate over the next million years. Following this, a number of snapshot simulations were identified and modeled using the IPSL_CM4_D GCM [*Marti et al.*, 2005], with the data then being downscaled to the regional level in order to provide, for example, input data for landscape evolution modeling. In addition, by deconvolving a series of characteristic timescales of CO_2 decay and their relative weights in the overall response, it may be possible to gain insights into carbon cycle processes such as their capacity for CO_2 uptake, the timescales over which they operate, and identify the emissions limits (if any) at which they, in effect, become saturated; the caveat in this respect being that there is no guarantee that statistically derived parameters map onto real world processes.

A limitation to the approach of representing the response of the long-term carbon cycle to a CO_2 perturbation as a pulse response function is that this type of analysis performs best when the system behaves in an approximately linear manner. However, carbon chemistry of the ocean is known to exhibit nonlinear behavior, reducing the accuracy of this method. This issue has been addressed by *Joos et al.* [1996], who used a combination of two pulse response functions in order to improve the accuracy of their results: one for the ocean mixed-layer which described the surface to deep-ocean mixing and one characterizing air-sea exchange. However, the method proposed by *Joos et al.* [1996] is not easily applied in our study, as our carbon cycle model allows ocean circulation to vary with time and includes a representation of the response of seafloor $CaCO_3$ sediments to atmospheric CO_2, which was not case for the models used in the original study.

Bearing in mind the previously employed utility of simple numerical models, the limited assessment of the importance of emissions size, but also caveats to making statistical fits, we present two main advances here. First, we create an ensemble of 1000–20,000 Pg C emissions experiments to explore how CO_2 sinks may weaken and saturate under high-end carbon releases in the *c*GENIE Earth system model. Second, we perform a multiexponential analysis on this ensemble to produce an impulse response function that captures the decay of the modeled atmospheric CO_2 perturbation and aids the analysis of the total emissions dependency of carbon sink dynamics. We also derive a convoluted version of this response function that can be used for rapid prediction of the atmospheric lifetime of future anthropogenic emissions. The paper is structured such that the *c*GENIE model and CO_2 scenarios are described in section 2, and the model results are presented in section 3. Section 4 discusses the results and their implications, and finally, the conclusions of this study are presented in section 5.

2. Methods

Our work is based around the "cGENIE" Earth system model [*Colbourn et al.*, 2013, *Ridgwell and Hargreaves*, 2007], for which we first (section 2.1) provide a summary description in conjunction with the acceleration technique devised to solve the long-term geochemical mass balance (itself described and evaluated in full in supporting information). We then describe the experimental setup and details of the carbon emissions experiments employed (2.2).

2.1. The cGENIE Earth System Model

We employ the carbon-centric version of the "GENIE" Earth system model (cGENIE). This is based on the efficient climate model of *Edwards and Marsh* [2005], comprising a 2-D Energy-Moisture Balance atmosphere, coupled to a 3-D frictional geostrophic ocean circulation model together with a dynamic-thermodynamic sea-ice component. Although lacking atmospheric dynamics and associated feedbacks, first-order estimates of the CO_2-climate feedback on ocean surface temperatures and ocean circulation can be made—both critical to projecting the millennial-scale uptake of excess CO_2 by the ocean. The version of cGENIE we employ also includes a representation of the global carbon cycle, including ocean biogeochemical cycling of dissolved inorganic carbon (DIC), alkalinity (ALK), and a single nutrient (PO_4) [*Ridgwell et al.*, 2007], geochemical interactions with calcium carbonate in marine sediments [*Ridgwell and Hargreaves*, 2007], and terrestrial weathering [*Colbourn et al.*, 2013]. The model is configured on a 36×36 equal-area horizontal grid with eight vertical levels in the ocean and is nonseasonally forced with insolation and wind stresses, both derived from observations. We select this particular configuration, rather than, e.g., a seasonal $36 \times 36 \times 16$ resolution such as evaluated by *Cao et al.* [2009] for direct comparison with previous analyses of CO_2 decay timescales of *Ridgwell and Hargreaves* [2007] and *Colbourn et al.* [2013].

cGENIE allows for one of a variety of possible representations of climate-weathering feedbacks to be employed [*Colbourn et al.*, 2013]. In all schemes, the terrestrial rock-weathering module calculates global fluxes of ALK and DIC from carbonate and silicate rock weathering and routes them to the coastal ocean in a pattern based on modern watersheds [*Edwards and Marsh*, 2005]. However, each scheme differs in the assumptions regarding what environmental factors modify the value of these fluxes. In this study, the fluxes are determined by, and are in feedback with, mean annual global land surface temperature (T). In our selected parameterization, inputs of calcium ions (Ca^{2+}) from carbonate (F_{CaCO_3}) and silicate (F_{CaSiO_3}) weathering take the form:

$$F_{CaCO_3} = F_{CaCO_3,0} \left(1 + k_{Ca} \left(T - T_0 \right) \right) \tag{1}$$

$$F_{CaSiO_3} = F_{CaSiO_3,0} \, e^{\frac{1000 E_a}{R T_0^2} \left(T - T_0 \right)} \tag{2}$$

where the 0 subscript represents an initial value of the parameter, k_{Ca} is an empirical constant (0.049), E_a is the activation energy for dissolution, and R is the molar gas constant. The temperature dependence of $CaCO_3$ (equation (1)) follows that used by *Berner* [1994], derived by correlating temperatures and bicarbonate concentrations of groundwater, while the relationship between silicate weathering and temperature (equation (2)) is based on laboratory studies of the impact of temperature on the dissolution of Ca and Mg silicates [*Brady*, 1991]. Here we have chosen to take the simplest possible approach and one mostly likely to lead to a decomposition into a set of separate decay timescales that might have some correspondence with geological processes, and we do not apply potential additional modifiers, e.g., runoff [*Berner et al.*, 1983] or terrestrial productivity [*Berner*, 1991]. The importance of the choice of weathering parameterization on the decay of atmospheric CO_2 on millennial timescales is analyzed and discussed in *Meissner et al.* [2012], who found that the CO_2 response of the temperature-only dependence part of the GEOCARB II parameterization [*Berner*, 1994] lay approximately in the middle of the responses for the other schemes they tested. A wider-ranging test of alternative parameterizations is provided by *Colbourn et al.* [2013], *Colbourn et al.* [2015], and *Colbourn* [2011].

In order to minimize the run time of the model, an acceleration technique was employed for solving the net impact of slow changes in weathering, CO_2 outgassing, and sedimentation. Briefly, once the relatively fast oceanic uptake processes have played out, and the effect of imbalance between (increased) rates of carbonate and silicate weathering and CO_2 out-gassing and burial of $CaCO_3$ in marine sediments start to dominate

Table 1. Summary of Accelerated cGENIE Model Experiments[a]

Set	Experiment	Total Emissions (Pg C)	Release Period (year)
Pulse series	1000	1000	0
	2000	2000	0
	3000	3000	0
	•	•	•
	•	•	•
	•	•	•
	•	•	•
	•	•	•
	20,000	20,000	0
Logistics series	1000	1000	2010–2810
	2000	2000	2010–2972
	3000	3000	2010–3050
	4000	4000	2010–3098
	5000	5000	2010–3132
	6000	6000	2010–3158
	8000	8000	2010–3196
	1000	10,000	2010–3223

[a](See supporting information for details and evaluation of acceleration methodology.)

the evolution of atmospheric CO_2, cGENIE periodically treats the ocean as a single box, solving explicitly for weathering and sedimentation on the model grid and then applying the mass difference uniformly throughout the ocean (preserving the tracer gradients). The underlying reasoning for this approach, as well as details regarding its detailed methodology, and an analysis of its fidelity in capturing projections of atmospheric CO_2 decay made using the full model, is provided as supporting information.

2.2. Model Spin-Up and CO_2 Scenarios

The cGENIE Earth system model was spun up in two stages following *Ridgwell and Hargreaves* [2007]: first, for 20 kyr with a "closed" $CaCO_3$ cycle where the flux of solutes to the ocean from terrestrial carbonate weathering is forced to equal the $CaCO_3$ burial rate, meaning that there is no gain or loss in ocean solutes. The second, 50 kyr spin-up, was with an "open" system configuration, meaning that ocean chemistry would adjust to any imbalance between inputs of solutes from weathering and losses from sediment burial, until the system came into balance. Total initial (preindustrial) weathering was split 50:50 between carbonate (5.59 Tmol yr^{-1}) and silicate weathering (5.59 Tmol yr^{-1}). To initially balance the silicate weathering component, a fixed volcanic CO_2 outgassing flux of (5.59 Tmol yr^{-1}) was specified. The annual mean land surface reference temperature (T_0 in equations (1) and (2)) was 8.5°C. This configuration is essentially the same as examined by *Colbourn et al.* [2013] and contrasted against alternative possible representations of long-term carbon cycle feedback, as well as by *Archer et al.* [2009] as part of a model intercomparison exercise.

Following on from this equilibrium state of global carbon cycling, two different series of emissions scenarios were carried out as summarized in Table 1. The first set consisted of an ensemble of 20 idealized pulse emissions experiments, in which the CO_2 release to the atmosphere occurred instantaneously at the start of year 0. Pulse emissions, as used previously by *Archer et al.* [2009], have been adopted here as it has been shown that the dominant control on the long-term response of atmospheric CO_2 is the total emissions rather than the rate of release [*Eby et al.*, 2009]. Our carbon emissions range is 1000–20,000 Pg C (Table 1). While remaining fossil fuel reserves that are currently potentially technically and economically viable have been estimated to be approximately 1000 Pg C, fossil fuel resources (where economic extraction may be feasible in the future) are estimated at ~4000 Pg C [*McGlade and Ekins*, 2015]. Our higher upper limit hence assumes future technoeconomic advances which make additional nonconventional resources such as methane clathrates (as high as 20–25,000 Pg C [*Rogner*, 1997]) available for extraction. Natural positive carbon cycle feedbacks involving for example permafrost would further amplify the effective total emissions. We also deliberately adopt a broad range of emissions so as to encompass geologically relevant carbon release estimates that run as high as ~13,000 Pg C or more for the transient Cenozoic global warming event, the Paleocene-Eocene Thermal Maximum [*Cui et al.*, 2011]. All ensemble members, including a zero-emission experiment as a control, were run for 1 Myr and used the accelerated version of cGENIE (see supporting information).

The second set of 1 Myr long experiments (Table 1) comprise emissions scenarios which follow observed historical atmospheric CO_2 concentrations from 1750 to year 2010 [*Meinshausen et al.*, 2011]. Emissions thereafter follow a logistic trajectory [*Winkelmann et al.*, 2015] to achieve cumulative emissions of 1000–10,000 Pg C between the years 2010 and ~3200 (Figure S1a in the supporting information). These experiments were also run out to 1 Myr and used the accelerated version of cGENIE.
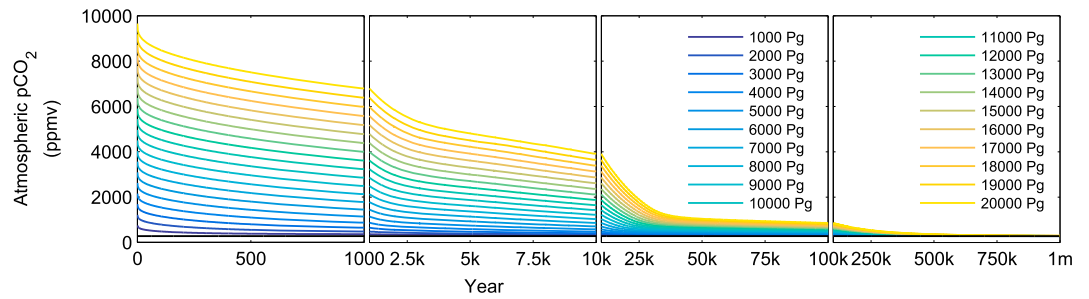
Figure 2. Atmospheric pCO$_2$ predicted by cGENIE for the pulse series scenarios (1000–20,000 Pg C). Preindustrial CO$_2$ concentrations are shown in black.

3. Results

3.1. Atmospheric Lifetime of Fossil Fuel CO$_2$

As expected, the atmospheric CO$_2$ perturbation in the model caused by each of the pulse emissions of 1000–20,000 Pg C is long-lived, taking hundreds of thousands of years to subside (Figures 2 and 3a). Even after 500 kyr, atmospheric pCO$_2$ has not yet returned to its preindustrial value, being 359.8 ppmv in the 20,000 Pg C scenario and 282.9 ppmv in the 1000 Pg C scenario, and is still gradually decreasing at a rate of 0.02 and 0.35 ppmv kyr^{-1}, respectively. This finding is consistent with previous studies which have found that an effectively complete recovery of atmospheric CO$_2$ takes more than 1 Myr for similar-sized emissions
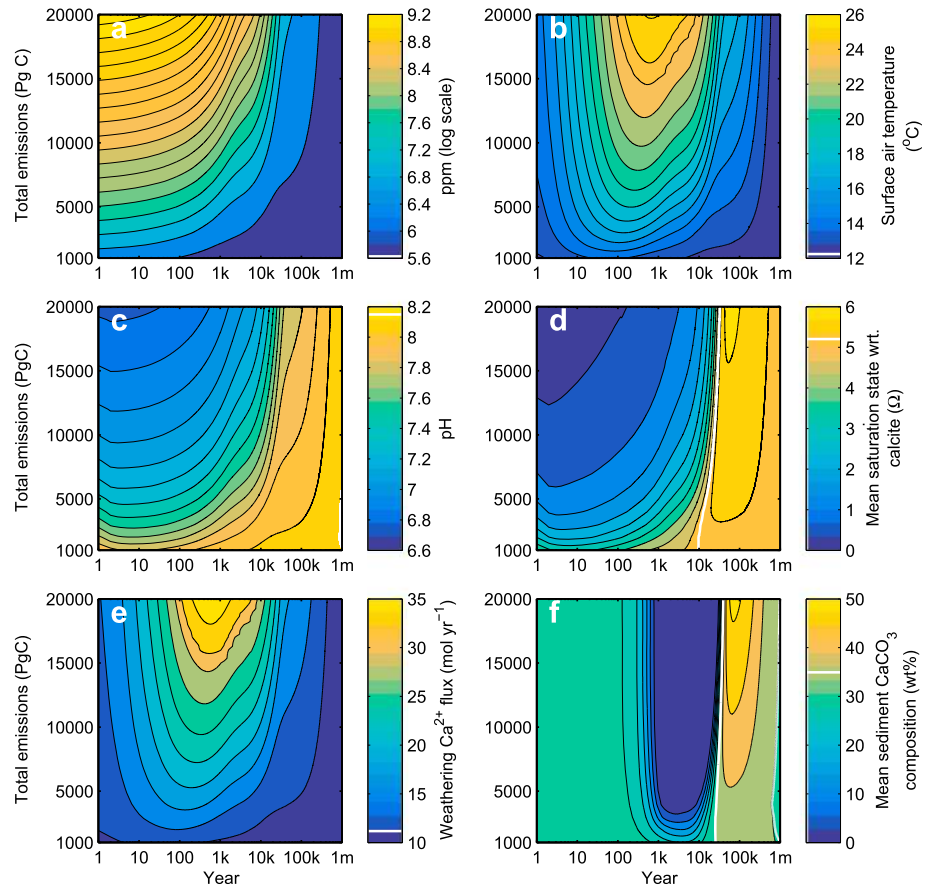
Figure 3. Response of climate to anthropogenic emissions for pulse series scenarios. Preindustrial state is shown as a white contour. (a) Atmospheric pCO$_2$, (b) mean global surface air temperature, (c) ocean surface pH, (d) ocean surface calcite saturation state, (e) global flux of Ca^{2+} to the ocean from terrestrial carbonate and silicate weathering, and (f) mean seafloor sediment CaCO$_3$ composition.
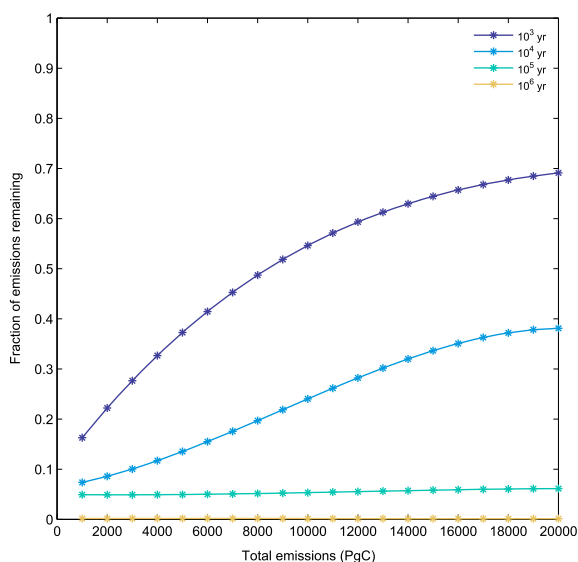
Figure 4. Fraction of emissions remaining in the atmosphere at 10^3, 10^4, 10^5, and 10^6 years as a function of total CO_2 emissions in Pg C for pulse series experiments. See supporting information (Table S2) for cubic coefficient values.

[*Colbourn et al.*, 2013; *Lenton and Britton*, 2006; *Walker and Kasting*, 1992]. Associated impacts such as warming (Figure 3b), ocean acidification (Figure 3c), and increased terrestrial carbonate and silicate weathering rates (Figure 3e) also last for hundreds of thousands of years. However, not all facets of the climate and carbon cycling recover at the same rates or even behave monotonically in post-peak emissions recovery (Figure 3).

Our results show that the lag between the peak atmospheric CO_2 concentration and the peak increase in mean surface air temperature increases with total emissions, ranging from ~60 years for the 1000 Pg C scenario up to ~700 years for the 20,000 Pg C release. The same pattern over time is also evident in the supply of Ca^{2+} to the ocean from terrestrial weathering (Figure 3e), due to its direct although nonlinear dependence on temperature in our chosen model configuration. As with atmospheric CO_2 concentration, surface air temperature, mean surface ocean pH, and weathering rate experience an initial perturbation following CO_2 emissions, which then subsides slowly over time. In contrast, mean global ocean surface saturation exhibits a more complex evolution with time. Initially, a period of reduced surface ocean calcite saturation state occurs (Figure 3d), which for the 6000–20,000 Pg C scenarios results in an interval of surface undersaturation on a global mean basis and which lasts for up to 3000 years under the highest emissions scenario. Subsequent to this, an overshoot in saturation state, caused by the imbalance between the input of solutes to the ocean from terrestrial weathering and marine sedimentation rates, occurs. Associated with the surface saturation changes is an overshoot in the $CaCO_3$ content of marine sediments (Figure 3f) caused by enhanced (above preindustrial levels) preservation of carbonate delivered to the sea floor. Conditions then relax toward their preindustrial states over several hundred thousand years but now from the opposite direction (of overshoot). The recovery of different elements of the carbonate system hence fundamentally diverges, with saturation state decoupled from pH (Figure 3d versus Figure 3c). This phenomenon is important in understanding the nature and biotic impacts of past ocean acidification [*Honisch et al.*, 2012] as well as future impacts on, e.g., tropical coral reefs [*Meissner et al.*, 2012].

Figure 4 shows the fraction of total emissions remaining in the atmosphere at various years as a cubic function of the total CO_2 emissions released. Supporting information provides full details of the analysis performed, as well as the cubic function (equation (S1)) and the coefficient values for the curves (Table S2). We find that the fraction of emissions remaining in the atmosphere is dependent on the amount of CO_2 released, with the fraction remaining on shorter timescales (10^3 and 10^4 years) being particularly sensitive. For these two timescales, this fraction increases with total emissions, due to the responses of a number of feedbacks in the system to the atmospheric CO_2 perturbation, which is discussed in more detail in section 4. As total emissions increase, the fraction remaining at 10^5 years increases slightly, while at the longest timescale of 10^6 years the fraction generally decreases. However, the relative change in the amount of CO_2 remaining in the atmosphere in response to emissions on the two longest timescales is trivial when compared to that of the shorter timescales.

3.2. Multiexponential Analysis of Atmospheric CO_2 Decay

A multiexponential function was fitted to the ensemble of atmospheric CO_2 decay curves generated in the pulse experiments (Figure 2), using the Matlab function NonLinearModel.fit, which took the form:

$$CO_2(t) = B + E \sum_{i=1}^{n} A_i \exp^{-(t-t_0)/\tau_i} \tag{3}$$
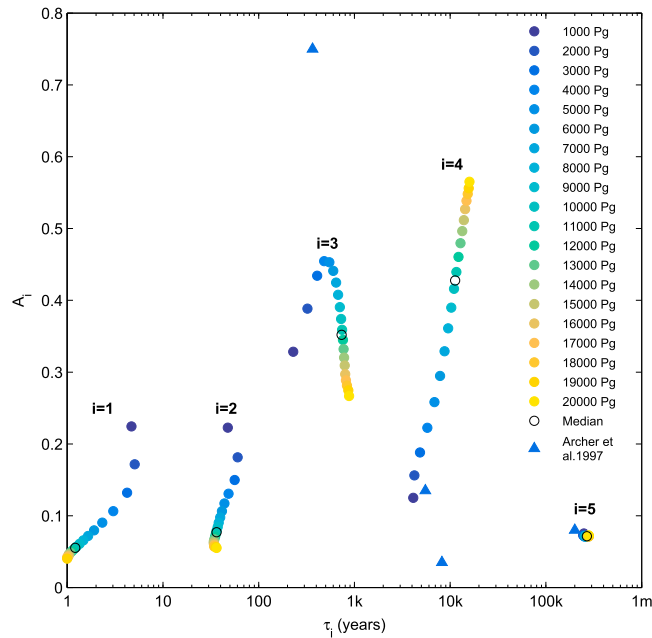
Figure 5. Change in fitting coefficient values (A_i and τ_i) for the five exponentials with total CO_2 emissions in Pg C for pulse series experiments. Also shown are the median values and the parameter values of *Archer et al.* [1997].

where $CO_2(t)$ is the atmospheric CO_2 concentration in ppmv at a given time (t) after the start of the decay curve t_0 (time 0 at the start of year 1), B is the preindustrial atmospheric CO_2 concentration (278 ppmv), and E is the total emissions released to the atmosphere in ppmv. Multiple numbers of exponentials were tested, with n ranging from 3 to 6. Each exponential term has two free parameters: τ_i is the timescale of decay and A_i represents the fraction of total emissions removed from the atmosphere over this timescale. Each curve fitting exercise was repeated 1000 times using different sets of randomly sampled initial coefficient values, establishing that the values identified for the coefficients are robust across a wide range of starting points. The curves were ranked using the Akaike Information Criterion (AIC), which measures the relative quality of the fit while favoring models with fewer parameters (the lowest score represents the best fit).

We found that five exponentials gave the optimal fit, having a lower AIC value and higher R-squared value (R^2) for all emissions scenarios compared with the 3- and 4-exponential fits. A number of previous studies have sought to capture the timescales of CO_2 decay by fitting four exponentials [*Archer et al.*, 1997; *Maier-Reimer and Hasselmann*, 1987]. In contrast, [*Colbourn*, 2011] tested fits of up to $n = 10$ on emissions of 1000 and 5000 Pg C. For the lower emissions scenario, he found that $n = 7$ was the optimal fit, whereas fewer curves ($n = 5$) gave the optimal fit for the scenario with higher emissions. In a recently published extension to this analysis, *Colbourn et al.* [2015] found that the sum of six exponential curves provided the best fit for a 1000 Pg C pulse emission. The results of our analysis is more in keeping with earlier studies as well as higher-end emissions of *Colbourn* [2011], and for the remainder of the results in this paper, we use $n = 5$.

The median values and range (minimum to maximum) for the five lifetimes (quoted as the e-folding time) across the full range of emissions scenarios are as follows: 1.2 years (1 to 5.1 years), 36 years (34 to 60 years), 730 years (230 to 880 years), 11 kyr (4 to 16 kyr), and 268 kyr (245 to 281 kyr). The exponentials represent the action of different processes or combinations of processes in the global carbon cycle that act to reduce the atmospheric CO_2 perturbation in the model (Figure 1). However, processes are unlikely to be individually captured by different terms due to overlaps in the timescales of their operation, an issue which is more likely to be a problem in interpreting the shorter timescale responses. We will nevertheless provide some possible interpretations of the processes that may in some way be associated with each of the terms later (section 4).

We find that the fitting parameters (A_i and τ_i) generally change in a nonlinear manner, and some of them demonstrate covariance in their relationship with total emissions, as evident in Figure 5. The first two exponentials decrease in efficiency (A_1 and A_2) as emissions increase, with a comparatively large step decrease for the scenarios with total emissions of up to 5000 Pg C. The timescales of these terms (τ_1 and τ_2) increase up to emissions of 2000 Pg C, before decreasing, with the lifetimes captured by the second term beginning to increase again for a 16,000 Pg C release.

The timescales of both the third and fourth exponentials (τ_3 and τ_4) monotonically increase with total emissions, but the responses of their efficiencies differ. For the third term (A_3), the efficiency increases up to emissions of
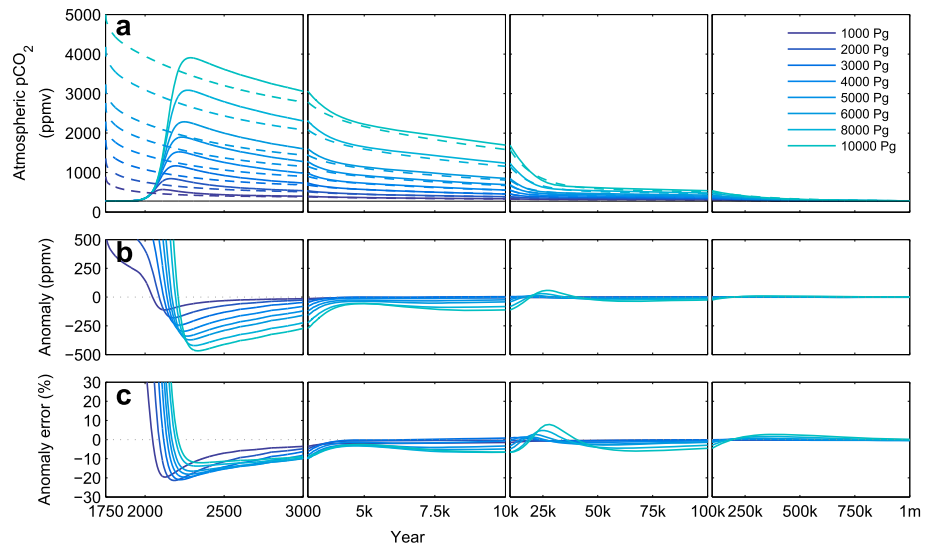
Figure 6. Logistics series scenarios for 1000–10,000 Pg C total emissions reproduced using the pulse response function (equation (4)). (a) Atmospheric pCO_2 predicted by cGENIE (solid line) and the pulse response function (dashed line). Preindustrial CO_2 concentrations are shown in black. (b) pCO_2 anomaly. (c) pCO_2 anomaly error. For initial residuals see supporting information (Figure S3).

4000 Pg C and then decreases as emissions increase further, potentially highlighting a threshold in the modeled carbon cycle response. In contrast, the fraction of CO_2 removed by the fourth exponential (A_4) monotonically increases with increasing emissions. As with the earlier terms, a relatively large change in the uptake fraction is seen for the lower emissions scenarios and as the emissions increase, the change in fractional uptake per Pg C increase declines.

Finally, and perhaps a little surprisingly, we find that A_5 varies only very little with total emissions. The time-scale of CO_2 removal (τ_5) also only increases very slightly as emissions increase and the relative change is trivial compared to the shorter timescale terms.

3.3. Convolution Analysis of Atmospheric CO_2 Decay

In order to create a single numerical description of CO_2 decay applicable across a range of total CO_2 emissions, we performed a regression analysis on the relationship between each fitting coefficient and total emissions. In this, we extended equation (3) and tested coefficients represented as linear, quadratic, and cubic functions of the total amount of carbon released. We then contrasted the projected decays of atmospheric CO_2 following pulse emissions of 1000–20,000 Pg C calculated using each possible variant (linear, quadratic, or cubic) of the response function to the equivalent atmospheric CO_2 response in cGENIE (pulse series experiments; Table 1). An F test was performed to assess which version of the regression model provided the best fit. For all the fitting coefficients except A_5 and τ_2, increasing the number of terms improved the model fit each time, significant at the 0.05 level. Use of cubic regression scaling factors for the fitting coefficients also decreased the root-mean-square error to 44 ppmv, from 53 ppmv for a quadratic fit, and from 136 ppmv for a linear fit. We therefore adopt the cubic coefficient description in the remainder of this paper, with the parameters listed in Table S3 in the supporting information. The full numerical function took the form:

$$CO_2(t) = B + E \sum_{i=1}^{n} \left(\alpha_i + \beta 1_i \mu + \beta 2_i \mu^2 + \beta 3_i \mu^3 \right) \exp^{-(t-t_0)/(\gamma_i + \delta 1_i \mu + \delta 2_i \mu^2 + \delta 3_i \mu^3)} \quad (4)$$

where μ is the carbon released at time 0 at the start of year 1 (Pg C).

We also applied this empirical form in a convolution analysis approach in order to improve the predictive capability of the response function for time-dependent emissions releases (logistics series experiments; Table 1). This is because the original response function (equation (3)) is based on the decay curve of an instantaneous pulse emission rather than a more drawn-out time-varying history of emissions as is occurring now and would characterize emissions across a geological event. To simulate the atmospheric
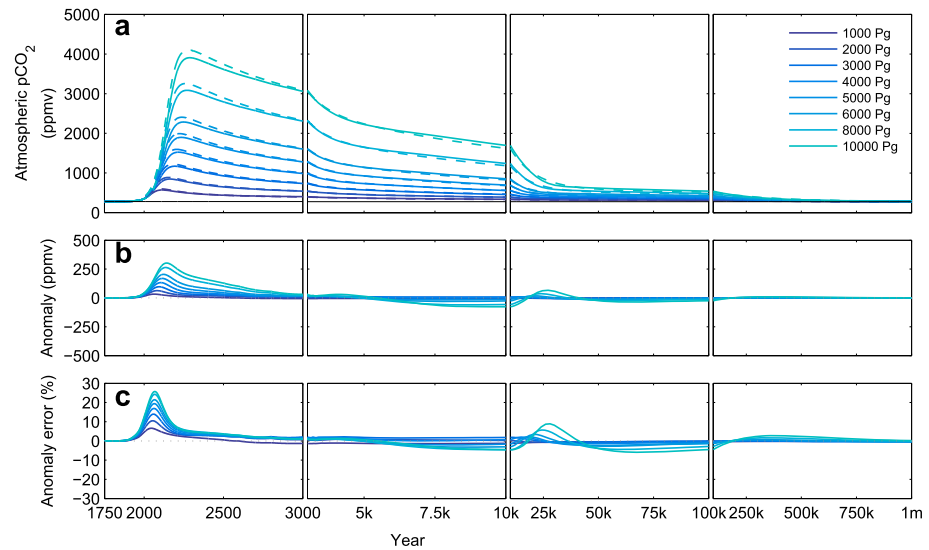
Figure 7. Logistics series scenarios for 1000–10,000 Pg C total emissions reproduced using the convoluted response function (equation (5)). (a) Atmospheric pCO$_2$ predicted by cGENIE (solid line) and the convoluted response function (dashed line). Preindustrial CO$_2$ concentrations are shown in black. (b) pCO$_2$ anomaly. (c) pCO$_2$ anomaly error.

response to the time-dependent emissions of the logistics series scenarios, CO$_2$ decay was modeled as a series of yearly pulse emissions using the response function. The CO$_2$ perturbations above preindustrial were then summed to give the progressive increase in atmospheric CO$_2$ over the emissions period:

$$\text{CO}_2(t) = B + \int_{t_0}^{t} q(x) \left(\sum_{i=1}^{n} A_i(\mu) \exp^{-(t-x)/\tau_i(\mu)} \right) dx \qquad (5)$$

where $q(x)$ is the release rate in ppmv yr^{-1}. The integral is over the period t_0 to t and the fitting coefficients are a cubic function of the total amount of carbon released (μ Pg C).

Depending on the emissions scenarios being used, both the pulse (equation (4)) and convoluted (equation (5)) response functions can be employed to predict the atmospheric CO$_2$ perturbation starting from initial preindustrial conditions (278 ppmv) or from already perturbed conditions, for example, following historical CO$_2$ emissions. For the latter, an additional step is required in which the decay of historical fossil fuel emissions to date is calculated and added to the projected CO$_2$ following future emissions, improving the prediction of the start of the curve for scenarios which include historical emissions. This approach was used in the following evaluation of the ability of the two impulse response functions to reproduce atmospheric pCO$_2$ for the logistics emissions scenarios. For the basic pulse response function, large residuals occur over the emissions period (the emissions occur from year 1750 to year 2810 for the 1000 Pg C emissions scenario and to year 3223 for the 10,000 Pg C scenario) due to the response function only being able to capture the decay of a pulse (Figures 6 and S3 in the supporting information). Response function and original model projections progressively converge after this, agreeing with the conclusion of Eby et $al.$ [2009] that the long-term response of atmospheric CO$_2$ is dependent on the total emissions rather than the rate of release. Overall, from the end of the respective emissions period (see Table 1 for years) onward percentage errors decline and are less than ±9% of cGENIE-modeled atmospheric pCO$_2$ in all scenarios (Figure 6c). The maximum percentage errors for this period for the 1000 and 10,000 Pg C scenarios are equivalent to 17.7 and 57.2 ppmv, respectively.

We find that the convoluted response function (equation (5)) much more closely reproduces the modeled atmospheric pCO$_2$ trajectories in the case of time-dependent emissions (Figure 7a), with the initial large residuals that occurred when using a single pulse response function (Figure S3 in the supporting information) now significantly reduced. CO$_2$ is still overpredicted during the interval of CO$_2$ release compared to the explicitly modeling (cGENIE) results (Figure 7)—a consequence of the cubic scaling coefficients being derived from an ensemble of experiments run with total instantaneous emissions starting at 1000 Pg C, which

represents a release rate averaged over 1 year some 2 orders of magnitude larger than current emissions. Nevertheless, maximum percentage errors in all scenarios are less than ±26% of atmospheric pCO_2, equivalent to 179.9 ppmv for the highest emissions scenario, and fall below ±9% by year 2200 (Figure 7c). For the 1000 and 10,000 Pg C scenarios, the maximum percentage errors beyond year 2200 are equivalent to 14.6 and 64.5 ppmv, respectively.

4. Discussion

By fitting a series of exponential decay curves to atmospheric pCO_2 data predicted using the cGENIE Earth system model, we can explore how the dynamics of removal of excess CO_2 from the atmosphere changes with cumulative CO_2 emissions. In theory, the principal carbon cycle process(es) most likely to be influencing the parameter values of each of the exponentials can be identified on the basis of a priori known timescales of these processes as well as the results of previous studies. However, in practice the exponentials will tend to represent the action of more than one process. In addition, changes in fitted parameter values with increasing emissions may reflect a change in the balance of processes encapsulated by a term, rather than a process(es) necessarily responding itself to emissions size. As in section 3, the values presented below are the median values for the fitting coefficients and the range of values (minimum to maximum) across the full range of emissions of 1000–20,000 Pg C.

4.1. Timescales and Magnitudes of CO_2 Removal

The two exponentials with the shortest timescales of years to decades (1.2 and 36 yrs) likely reflect a range of processes involving air-sea gas transfer, reaction of CO_2 with seawater, and invasion of CO_2 into the upper water column. Particularly in light of their very similar response to increasing total emissions in τ_i versus A_i space (Figure 5), we regard them as inseparable with respect to their interpretation. While the third exponential is separated by an order of magnitude in timescale from the second, the existence of a common inflection point around 4000–5000 Pg C in all first three terms suggests that again, distinct or independent processes are not being separated by the exponential deconvolution. The 730 yr timescale of the third term suggests that ocean circulation and CO_2 transport away from the surface is involved, but the nature of this may not be separable from the shorter timescale terms.

One might more usefully then combine terms 1–3 and ascribe this sink to "ocean" (primarily physical transport) processes and the carbonate buffering capacity of ocean waters. Across the range of pulse emissions (1000–20,000 Pg C), the equilibrium partitioning of CO_2 between ocean and atmosphere is such that approximately 50% (6% + 8% + 35%) is removed (range: 36–80%), leaving ~50% (20–64%) in the atmosphere. This estimated value for the CO_2 sink capacity of the ocean is lower than some previous estimates, which have estimated that the ocean may be able to store ~60–80% of fossil fuel emissions [*Archer and Brovkin*, 2008; *Archer et al.*, 1997; *Ridgwell and Hargreaves*, 2007]. However, as identified previously [*Archer*, 2005; *Archer et al.*, 1998, 2009], the fraction removed by the ocean depends on total emissions, and the value quoted here is an average across a wide range of emissions. Our findings can be reconciled with previous studies by considering how the lifetimes and values of fractional uptake depend on emissions, as we discuss in section 4.2.

We have rather more confidence that the final two terms represent relatively distinct (geological) processes. First, the behavior of the fourth and fifth exponentials is very different both from each other as well as from the first three exponentials (Figure 5), i.e., their behavior with increasing emissions size is unlikely to be a statistical artefact of the CO_2 decay curve fitting. The characteristics of both the final two terms are also broadly consistent with previous studies carried out with different analysis methods and often using very different ocean model components.

Across the range of modeled emissions, the fourth exponential has a median timescale of 11 kyr and accounts for the removal of 43% (12–57%) of the excess CO_2 added to the atmosphere. A study by *Ridgwell and Hargreaves* [2007] characterized the individual operating timescales of seafloor neutralization and terrestrial neutralization for a 4000 Pg C release, obtaining values of 1.7 kyr and 8.3 kyr, respectively. We therefore infer that the fourth timescale in our study is likely to, at least partially, represent the combined action of these processes, as we obtain a response time (τ_4) of 5.8 kyr for an equivalent total CO_2 release.

The fifth and final exponential represents increased silicate weathering. Previous studies have often not modeled long-term silicate weathering explicitly but instead assume a relaxation timescale for this process of, for example, 200 kyr [*Archer et al.*, 1997, 1998] or 400 kyr [*Archer*, 2005]. However, using a box model, *Lenton and Britton* [2006] made a half-life estimate of ~200 kyr for silicate weathering following emissions of ~1100–15,000 Pg C in model simulations run for 1 Myr. This value is broadly similar to the timescale for the fifth and final exponential in our study of 245–278 kyr for the same range of emissions. Our modeled fraction of CO_2 that is neutralized on this timescale is 7% (7–8%), in good agreement with previous estimates of 7–8% deduced from the CO_2 residual in experiments lacking an explicit representation of the feedback [*Archer et al.*, 1997, 1998; *Ridgwell and Hargreaves*, 2007].

4.2. The Importance of CO_2 Emissions Size and Buffer Depletion

The values of the fractions and timescales of CO_2 uptake in the model captured by the five exponentials vary with total emissions. These trends are related to the marine carbon feedbacks in the Earth system that is included in the *c*GENIE model. For example, a range of modeling studies have recognized that the proportional uptake by the ocean of an atmospheric CO_2 anomaly is a function of the size of that anomaly (magnitude of total emissions) [*Archer*, 2005; *Archer et al.*, 1998; *Eby et al.*, 2009; *Lenton and Britton*, 2006]. One reason for this is that the efficiency of ocean invasion decreases as emissions increase due to a series of well-established carbon feedbacks. The first feedback links CO_2 uptake and temperature as a result of the reduction of the solubility of gaseous CO_2 in sea water with increasing temperature [*Zeebe and Wolf-Gladrow*, 2001]. The second feedback relates to the decline in the strength of carbonate ion buffering of seawater and an increasing "Revelle factor" [*Zeebe and Wolf-Gladrow*, 2001] as atmospheric CO_2 concentrations increase. In other words, the proportional uptake by the ocean of a unit excess of atmospheric CO_2 declines as atmospheric CO_2 (and total emissions) increases [*Sarmiento et al.*, 1995]. Third, differential warming of the surface versus depth will increase stratification and tend to decrease the strength of ocean overturning circulation and hence CO_2 transport to depth. The general decline in the fractional importance of all three initial terms (A_1, A_2, and A_3) is consistent with these processes. The initial strengthening of importance of the third term and increase in value of A_3 for total emissions up to ~4000 Pg C in size may perhaps paradoxically, be related to the progressive collapse of the Atlantic Meridional Overturning Circulation (AMOC). Although collapse of AMOC in the model would inhibit transport of dissolved CO_2 into the deep ocean from the North Atlantic surface, a small positive feedback arises from reduced CO_2 uptake associated with a weakening of the AMOC as carbon delivered to depth via the biological pump becomes more effectively isolated in the deep North Atlantic [*Montenegro et al.*, 2007; *Zickfeld et al.*, 2008]. In other words, high carbon storage due to a more efficient biological pump in the North Atlantic may at least temporarily, outweigh a weaker solubility pump (e.g., see *Chikamoto et al.* [2008]). The timescales of the first two terms (τ_1 and τ_2) generally decrease with total emissions, while those of the third term (τ_3) increase with total emissions, although the inflection following the initial increase in timescale of τ_1 and τ_2 is not readily ascribed any physical reason and may reflect a shift in the statistical fit associated with the more pronounced inflection in A_3. Overall, analysis of the first three terms is a good illustration of the difficulties in ascribing specific process to statistical terms. However, the inflection in the parameter space trajectories of all three terms around 4000 Pg C (Figure 5) may well be driven by a real physical phenomenon (AMOC collapse in the model).

Previous studies have estimated that the ocean removes 60–80% of total emissions of 1000–5000 Pg C (higher for higher emissions) [*Archer*, 2005; *Archer et al.*, 1997], a fraction that declines to ~30% for 15,000 Pg C [*Lenton*, 2006]. This is in broadly good agreement with the range of values for the estimated ocean fraction (sum of A_1, A_2, and A_3) derived here, which vary from 80% to 42% for 1000 and 15,000 Pg C, respectively. The approximate timescale of ocean uptake of up to ~550 years for emissions of 1000–5000 Pg C (longer for higher emissions) is also close to previous estimates of 200–450 years [*Archer et al.*, 1997, 1998]. The difference here and the reason for our slightly longer estimate may simply reflect the lack of a climate feedback and hence of a circulation slow-down in the analysis of *Archer et al.* [1997, 1998].

The values of A_4 and τ_4 increase with emissions size, as they are likely affected by the combined responses of seafloor and terrestrial $CaCO_3$ neutralization to the modeled atmospheric CO_2 perturbation. This is partly a consequence of the fact that the erodable deep-sea sediment $CaCO_3$ reservoir becomes depleted in the

higher emissions scenarios (≥5000 Pg C) as first recognized by *Archer et al.* [1997, 1998] and further elucidated by *Goodwin and Ridgwell* [2010]. Once the available surface and near-surface sediment $CaCO_3$ is depleted, the further uptake of atmospheric CO_2 by the process of seafloor $CaCO_3$ neutralization ceases. However, at the same time, with increasing total emissions, the imbalance between terrestrial weathering rates and deep-sea carbonate burial also increases with a more rapid supply of weathering solutes to the ocean. The result is that the characteristic fraction (A_4) and timescale (τ_4) both progressively increase with total emissions but do not exhibit any obvious threshold behavior in the region of 5000 Pg C emissions, which is the point at which the erodible deep-sea $CaCO_3$ is projected to become exhausted [*Archer et al.*, 1997; *Goodwin and Ridgwell*, 2010]. The lack of an identifiable statistically recoverable transition as the seafloor $CaCO_3$ neutralization sink is exhausted cautions against separating seafloor and terrestrial neutralization processes (e.g., as per *Ridgwell and Hargreaves* [2007]), or at least, cautions against overinterpreting the importance of exhausting the former.

Combining the two processes of seafloor and terrestrial $CaCO_3$ neutralization, *Ridgwell and Hargreaves* [2007] estimated the total CO_2 uptake to be ~26%, which aligns well with our results when taking into account emissions size, with our 4000 Pg C scenario value for A_3 being 22%. *Archer et al.* [1997] projected that, for emissions of 900–4500 Pg C, these two processes account for the removal of 13–23% of total emissions from the atmosphere over periods of 5.5–6.8 kyr and 8.2 kyr. Here the comparable range for total emissions of 1000–5000 Pg C is somewhat higher at 12–26%, but with a combined *e*-folding timescale ranging from 4 to 6.9 kyr, i.e., slightly shorter than found by *Archer et al.* [1997]. These differences can be explained because the modeling approach used by *Archer et al.* [1997] did not include the feedbacks that result from increased atmospheric CO_2 on ocean circulation, meaning that ocean invasion will tend to proceed more rapidly, and hence, interactions with deep-sea sediments occur sooner. Our findings are also consistent with the work of *Goodwin and Ridgwell* [2010], who compared the ocean-atmosphere partitioning of CO_2 emissions following $CaCO_3$ sediment equilibration as calculated by an analytical method and found that ~7–33% of total emissions were removed from the atmosphere by the equilibrated $CaCO_3$ sediment feedback and that this fraction increases as total emissions increase.

Finally, and perhaps a little surprisingly, we find that A_5 varies only very little with total emissions, as the relative efficiency of CO_2 removal by the four faster mechanisms in the model tend to compensate for each other, meaning that the atmospheric fraction of total emissions that remains to be neutralized by increased weathering is approximately the same in all scenarios. This is consistent with previous work that found that the fraction of emissions remaining in the atmosphere beyond 100 kyr (and hence that left to be neutralized by silicate weathering) to be relatively unaffected by total emissions [*Lenton and Britton*, 2006]. The timescale of CO_2 removal (τ_5) can be seen to increase slightly with total emissions, but again, the relative change is small particularly compared to that of, e.g., τ_3 and τ_4 (Figure 5).

5. Conclusions

We have carried out a series of instantaneous pulse emissions of 1000–20,000 Pg C in an Earth system model to highlight the long-term decay dynamics of a CO_2 perturbation. In a multiexponential analysis of this model ensemble we have assessed how the characteristics of the CO_2 decay changes with total emissions. We find that for the shorter (<1000 year) timescales of decay, which likely reflect a range of ocean circulation, carbonate chemistry, and air-sea gas exchange processes, the fractional removal of excess CO_2 from the atmosphere depends strongly and nonlinearly on total emissions. This illustrates how the buffering and CO_2 uptake by the ocean on anthropogenic timescales progressively saturates with increasing total emissions. To compensate, excess CO_2 removal from the atmosphere due to carbonate weathering and burial progressively increases in importance with increasing emissions, but at a progressively slower rate for higher total emissions. In contrast to the ocean dynamics and carbonate weathering processes, we find that the *e*-folding timescale for the silicate feedback as well as its relative importance in removal of excess CO_2 from the atmosphere is almost independent of emissions size.

We created an impulse response function (pulse emissions—equation (4) and time-dependent emissions—equation (5), both using coefficient values in Table S3 in the supporting information) which is able to reproduce model-predicted atmospheric CO_2 data following pulse emissions of up to 20,000 Pg C. Our function provides a simple and practical tool for rapidly projecting the atmospheric lifetime of a CO_2 emission. Its

primary advantage is that it can be used across a large range of emissions sizes and rates of release and removes the need for long simulations using computationally expensive models.

However, we have omitted the role of the terrestrial biosphere from our analysis and furthermore focused on a relatively simple and global mean function linking weathering rates and climate. Future work should explore uncertainties in the strength and dynamical characteristics of the silicate weathering feedback, as well as accounting for the role of the organic carbon cycle.

Code Availability

Code for the pulse and convoluted response functions is included in 2 Python scripts (Lordetal_sfts01.py, Lordetal_sfts02.py) as supporting information. The data used in this paper are available from Natalie Lord (Natalie.Lord@bristol.ac.uk).

References

Archer, D. (2005), Fate of fossil fuel CO_2 in geologic time, *J. Geophys. Res.*, *110*, C09S05, doi:10.1029/2004JC002625.

Archer, D., and V. Brovkin (2008), The millennial atmospheric lifetime of anthropogenic CO_2, *Clim. Change*, *90*(3), 283–297, doi:10.1007/s10584-008-9413-1.

Archer, D., and A. Ganopolski (2005), A movable trigger: Fossil fuel CO_2 and the onset of the next glaciation, *Geochem. Geophys. Geosyt.*, *6*, Q05003, doi:10.1029/2004GC000891.

Archer, D., H. Kheshgi, and E. Maier-Reimer (1997), Multiple timescales for neutralization of fossil fuel CO_2, *Geophys. Res. Lett.*, *24*(4), 405–408, doi:10.1029/97GL00168.

Archer, D., H. Kheshgi, and E. Maier-Reimer (1998), Dynamics of fossil fuel CO_2 neutralization by marine $CaCO_3$, *Global Biogeochem. Cycles*, *12*(2), 259–276, doi:10.1029/98GB00744.

Archer, D., et al. (2009), Atmospheric lifetime of fossil fuel carbon dioxide, *Annu. Rev. Earth Planet. Sci.*, *37*, 117–134, doi:10.1146/annurev.earth.031208.100206.

Bains, S., R. D. Norris, R. M. Corfield, and K. L. Faul (2000), Termination of global warmth at the Palaeocene/Eocene boundary through productivity feedback, *Nature*, *407*(6801), 171–174, doi:10.1038/35025035.

Berger, A., and M. F. Loutre (1996), Modelling the climate response to astronomical and CO_2 forcings, *C. R. Acad. Sci., Ser. IIa*, *323*(1), 1–16.

Berger, A., and M. F. Loutre (2002), An exceptionally long interglacial ahead?, *Science*, *297*(5585), 1287–1288, doi:10.1126/science.1076120.

Berner, R. A. (1990), Atmospheric carbon dioxide levels over phanerozoic time, *Science*, *249*(4975), 1382–1386, doi:10.1126/science.249.4975.1382.

Berner, R. A. (1991), A model for atmospheric CO_2 over phanerozoic time, *Am. J. Sci.*, *291*(4), 339–376, doi:10.2475/ajs.291.4.339.

Berner, R. A. (1994), 3GEOCARB II—A revised model of atmospheric CO_2 over phanerozoic time, *Am. J. Sci.*, *294*(1), 56–91, doi:10.2475/ajs.294.1.56.

Berner, R. A. (1999), A new look at the long-term carbon cycle, *GSA Today*, *9*(11), 1–6.

Berner, R. A., and K. Caldeira (1997), The need for mass balance and feedback in the geochemical carbon cycle, *Geology*, *25*(10), 955–956, doi:10.1130/0091-7613(1997)025.

Berner, R. A., A. C. Lasaga, and R. M. Garrels (1983), The carbonate-silicate geochemical cycle and its effect on atmospheric carbon dioxide over the past 100 million years, *Am. J. Sci.*, *283*(7), 641–683, doi:10.2475/ajs.283.7.641.

BIOCLIM (2001), *Deliverable D3: Global Climatic Features Over the Next Million Years and Recommendation for Specific Situations to Be Considered*, ANDRA, Parc de la Croix Blanche, Châtenay-Malabry, France. [Available at www.andra.fr/bioclim/documentation.]

Brady, P. V. (1991), The effect of silicate weathering on global temperature and atmospheric CO_2, *J. Geophys. Res.*, *96*(B11), 18,101–18,106, doi:10.1029/91JB01898.

Cao, L., et al. (2009), The role of ocean transport in the uptake of anthropogenic CO_2, *Biogeosciences*, *6*(3), 375–390, doi:10.5194/bg-6-375-2009.

Chikamoto, M. O., K. Matsumoto, and A. Ridgwell (2008), Response of deep-sea $CaCO3$ sedimentation to Atlantic meridional overturning circulation shutdown, *J. Geophys. Res.*, *113*, G03017, doi:10.1029/2007JG000669.

Colbourn, G. (2011), Weathering effects on the carbon cycle in an Earth system model, PhD thesis, Univ. of East Anglia, UK, Norwich, U. K. [Available at www.ueaeprints.uea.ac.uk/34242/.]

Colbourn, G., A. Ridgwell, and T. M. Lenton (2013), The Rock Geochemical Model (RokGeM) v0.9, *Geosci. Model Dev.*, *6*(5), 1543–1573, doi:10.5194/gmd-6-1543-2013.

Colbourn, G., A. Ridgwell, and T. Lenton (2015), The time scale of the silicate weathering negative feedback on atmospheric CO_2, *Global Biogeochem. Cycles*, *29*, 583–596, doi:10.1002/2014GB005054.

Cui, Y., L. R. Kump, A. J. Ridgwell, A. J. Charles, C. K. Junium, A. F. Diefendorf, K. H. Freeman, N. M. Urban, and I. C. Harding (2011), Slow release of fossil carbon during the Palaeocene-Eocene Thermal Maximum, *Nat. Geosci.*, *4*(7), 481–485, doi:10.1038/Ngeo1179.

Eby, M., K. Zickfeld, A. Montenegro, D. Archer, K. J. Meissner, and A. J. Weaver (2009), Lifetime of anthropogenic climate change: Millennial time scales of potential CO_2 and surface temperature perturbations, *J. Clim.*, *22*(10), 2501–2511, doi:10.1175/2008jcli2554.1.

Edwards, N., and R. Marsh (2005), Uncertainties due to transport-parameter sensitivity in an efficient 3-D ocean-climate model, *Clim. Dyn.*, *24*(4), 415–433, doi:10.1007/s00382-004-0508-8.

Gallee, H., J. P. Vanypersele, T. Fichefet, C. Tricot, and A. Berger (1991), Simulation of the last glacial cycle by a coupled, sectorially averaged climate-ice sheet model .1. The climate model, *J. Geophys. Res.*, *96*(D7), 13,139–13,161, doi:10.1029/91JD00874.

Gallee, H., J. P. Vanypersele, T. Fichefet, I. Marsiat, C. Tricot, and A. Berger (1992), Simulation of the last glacial cycle by a coupled, Sectorially averaged climate-ice sheet model. 2. Response to Insolation and CO_2 Variations, *J. Geophys. Res.*, *97*(D14), 15,713–15,740.

Goodwin, P., and A. Ridgwell (2010), Ocean–atmosphere partitioning of anthropogenic carbon dioxide on multimillennial timescales, *Global Biogeochem. Cycles*, *24*, GB2014, doi:10.1029/2008GB003449.

Honisch, B., et al. (2012), The geological record of ocean acidification, *Science*, *335*(6072), 1058–1063, doi:10.1126/science.1208277.

Hunter, S. J., D. S. Goldobin, A. M. Haywood, A. Ridgwell, and J. G. Rees (2013), Sensitivity of the global submarine hydrate inventory to scenarios of future climate change, *Earth Planet. Sci. Lett.*, *367*, 105–115, doi:10.1016/j.epsl.2013.02.017.

Jenkyns, H. C. (1980), Cretaceous anoxic events—From continents to oceans, *J. Geol. Soc. London*, *137*, 171–188, doi:10.1144/gsjgs.137.2.0171.

Joos, F., M. Bruno, R. Fink, U. Siegenthaler, T. F. Stocker, and C. LeQuere (1996), An efficient and accurate representation of complex oceanic and biospheric models of anthropogenic carbon uptake, *Tellus B*, *48*(3), 397–417, doi:10.1034/j.1600-0889.1996.t01-2-00006.x.

Joos, F., I. C. Prentice, S. Sitch, R. Meyer, G. Hooss, G. K. Plattner, S. Gerber, and K. Hasselmann (2001), Global warming feedbacks on terrestrial carbon uptake under the Intergovernmental Panel on Climate Change (IPCC) emission scenarios, *Global Biogeochem. Cycles*, *15*(4), 891–907, doi:10.1029/2000GB001375.

Joos, F., et al. (2013), Carbon dioxide and climate impulse response functions for the computation of greenhouse gas metrics: A multi-model analysis, *Atmos. Chem. Phys.*, *13*(5), 2793–2825, doi:10.5194/acp-13-2793-2013.

Kohler, P., H. Fischer, G. Munhoven, and R. E. Zeebe (2005), Quantitative interpretation of atmospheric carbon records over the last glacial termination, *Global Biogeochem. Cycles*, *19*, GB4020, doi:10.1029/2004GB002345.

Lawrence, D. M., A. G. Slater, and S. C. Swenson (2012), Simulation of present-day and future permafrost and seasonally frozen ground conditions in CCSM4, *J. Clim.*, *25*(7), 2207–2225, doi:10.1175/Jcli-D-11-00334.1.

Leckie, R. M., T. J. Bralower, and R. Cashman (2002), Oceanic anoxic events and plankton evolution: Biotic response to tectonic forcing during the mid-Cretaceous, *Paleoceanography*, *17*(3), 1041, doi:10.1029/2001PA000623.

Lenton, T. M. (2006), Climate change to the end of the millennium—An editorial review essay, *Clim. Change*, *76*(1–2), 7–29, doi:10.1007/s10584-005-9022-1.

Lenton, T. M., and C. Britton (2006), Enhanced carbonate and silicate weathering accelerates recovery from fossil fuel CO_2 perturbations, *Global Biogeochem. Cycles*, *20*, GB3009, doi:10.1029/2005GB002678.

Maier-Reimer, E., and K. Hasselmann (1987), Transport and storage of CO_2 in the ocean—An inorganic ocean-circulation carbon cycle model, *Clim. Dyn.*, *2*(2), 63–90, doi:10.1007/Bf01054491.

Marti, O., et al. (2005), *The New IPSL Climate System Model: IPSL-CM4*, *Note du Pôle de Modélisation*, vol. 26, Institut Pierre Simon Laplace, Paris.

McGlade, C., and P. Ekins (2015), The geographical distribution of fossil fuels unused when limiting global warming to 2°C, *Nature*, *517*(7533), 187–U143, doi:10.1038/Nature14016.

Meinshausen, M., et al. (2011), The RCP greenhouse gas concentrations and their extensions from 1765 to 2300, *Clim. Change*, *109*(1–2), 213–241, doi:10.1007/s10584-011-0156-z.

Meissner, K. J., B. I. McNeil, M. Eby, and E. C. Wiebe (2012), The importance of the terrestrial weathering feedback for multimillennial coral reef habitat recovery, *Global Biogeochem. Cycles*, *26*, GB3017, doi:10.1029/2011GB004098.

Montenegro, A., V. Brovkin, M. Eby, D. Archer, and A. J. Weaver (2007), Long term fate of anthropogenic carbon, *Geophys. Res. Lett.*, *34*, L19707, doi:10.1029/2007GL030905.

Penman, D. E., B. Honisch, R. E. Zeebe, E. Thomas, and J. C. Zachos (2014), Rapid and sustained surface ocean acidification during the Paleocene-Eocene Thermal Maximum, *Paleoceanography*, *29*, 357–369, doi:10.1002/2014pa002621.

Ridgwell, A., and J. C. Hargreaves (2007), Regulation of atmospheric CO_2 by deep-sea sediments in an Earth system model, *Global Biogeochem. Cycles*, *21*, GB2008, doi:10.1029/2006GB002764.

Ridgwell, A., and D. N. Schmidt (2010), Past constraints on the vulnerability of marine calcifiers to massive carbon dioxide release, *Nat. Geosci.*, *3*(3), 196–200, doi:10.1038/Ngeo755.

Ridgwell, A., J. C. Hargreaves, N. R. Edwards, J. D. Annan, T. M. Lenton, R. Marsh, A. Yool, and A. Watson (2007), Marine geochemical data assimilation in an efficient Earth system model of global biogeochemical cycling, *Biogeosciences*, *4*(1), 87–104, doi:10.5194/bg-4-87-2007.

Rogner, H. H. (1997), An assessment of world hydrocarbon resources, *Annu. Rev. Energy Environ.*, *22*, 217–262, doi:10.1146/annurev.energy.22.1.217.

Sarmiento, J. L., J. C. Orr, and U. Siegenthaler (1992), A perturbation simulation of CO_2 uptake in an ocean general-circulation model, *J. Geophys. Res.*, *97*(C3), 3621–3645, doi:10.1029/91JC02849.

Sarmiento, J. L., C. Lequere, and S. W. Pacala (1995), Limiting future atmospheric carbon dioxide, *Global Biogeochem. Cycles*, *9*(1), 121–137, doi:10.1029/94GB01779.

Schimel, D., B. B. Stephens, and J. B. Fisher (2015), Effect of increasing CO_2 on the terrestrial carbon cycle, *Proc. Natl. Acad. Sci. U.S.A.*, *112*(2), 436–441, doi:10.1073/pnas.1407302112.

Schlanger, S. O., and H. C. Jenkyns (1976), Cretaceous oceanic anoxic events: Causes and consequences, *Geol. Mijnbouw*, *55*(3–4), 179–184.

Sitch, S., et al. (2008), Evaluation of the terrestrial carbon cycle, future plant geography and climate-carbon cycle feedbacks using five Dynamic Global Vegetation Models (DGVMs), *Global Change Biol.*, *14*(9), 2015–2039, doi:10.1111/j.1365-2486.2008.01626.x.

Stone, E. J., D. J. Lunt, I. C. Rutt, and E. Hanna (2010), Investigating the sensitivity of numerical model simulations of the modern state of the Greenland ice-sheet and its future response to climate change, *Cryosphere*, *4*(3), 397–417, doi:10.5194/tc-4-397-2010.

Turley, C., et al. (2010), Carbon uptake, transport and storage by oceans and the consequences of change in carbon capture and storage (CCS), in *Issues in Environmental Science and Technology (IEST)*, edited by R. M. Harrison and R. E. Hester, pp. 240–284, Royal Society of Chemistry, Cambridge, U. K.

Tyrrell, T., J. G. Shepherd, and S. Castle (2007), The long-term legacy of fossil fuels, *Tellus B*, *59*(4), 664–672, doi:10.1111/j.1600-0889.2007.00290.x.

van der Sleen, P., P. Groenendijk, M. Vlam, N. P. R. Anten, A. Boom, F. Bongers, T. L. Pons, G. Terburg, and P. A. Zuidema (2015), No growth stimulation of tropical trees by 150 years of CO_2 fertilization but water-use efficiency increased, *Nat. Geosci.*, *8*(1), 24–28, doi:10.1038/Ngeo2313.

Walker, J. C. G., and J. F. Kasting (1992), Effects of fuel and forest conservation on future levels of atmospheric carbon dioxide, *Global Planet. Change*, *97*(3), 151–189, doi:10.1016/0921-8181(92)90009-Y.

Walker, J. C. G., P. B. Hays, and J. F. Kasting (1981), A negative feedback mechanism for the long-term stabilization of Earths surface-temperature, *J. Geophys. Res.*, *86*(C10), 9776–9782, doi:10.1029/JC086ic10p09776.

Winkelmann, R., A. Levermann, A. Ridgwell, and K. Caldeira (2015), Combustion of available fossil-fuel resources sufficient to eliminate the Antarctic Ice Sheet, *Sci. Adv.*, *1*(8), e1500589, doi:10.1126/sciadv.1500589.

Zachos, J. C., and G. R. Dickens (2000), An assessment of the biogeochemical feedback response to the climatic and chemical perturbations of the LPTM, *GFF*, *122*, 188–189.

Zeebe, R. E. (2013), What caused the long duration of the Paleocene-Eocene Thermal Maximum?, *Paleoceanography*, *28*, 440–452, doi:10.1002/Palo.20039.

Zeebe, R. E., and D. A. Wolf-Gladrow (2001), *CO in Seawater: Equilibrium, Kinetics, Isotopes*, vol. xiii, p. 346, Elsevier, Amsterdam.

Zeebe, R. E., and J. C. Zachos (2013), Long-term legacy of massive carbon input to the Earth system: Anthropocene versus Eocene, *Philos. Trans. R. Soc., A*, *371*, 20120006, doi:10.1098/Rsta.2012.0006.

Zickfeld, K., M. Eby, and A. J. Weaver (2008), Carbon-cycle feedbacks of changes in the Atlantic meridional overturning circulation under future atmospheric CO_2, *Global Biogeochem. Cycles*, *22*, GB3024, doi:10.1029/2007GB003118.